Inorganic Chemistry

Article

pubs.acs.org/IC

$TM_7TM'_6B_8$ (TM = Ta, Nb; TM' = Ru, Rh, Ir): New Compounds with $[B_6]$ Ring Polyanions

Qiang Zheng,[†,‡,§] Miroslav Kohout,[†] Roman Gumeniuk,[†] Nikolay Abramchuk,[†] Horst Borrmann,[†] Yurii Prots,[†] Ulrich Burkhardt,[†] Walter Schnelle,[†] Lev Akselrud,[†] Hui Gu,[‡] Andreas Leithe-Jasper,[†] and Yuri Grin*[,†]

[†]Max-Planck-Institut für Chemische Physik fester Stoffe, Nöthnitzer Str. 40, 01187 Dresden, Germany

[‡]State Key Laboratory of High Performance Ceramics and Superfine Microstructures, Shanghai Institute of Ceramics, Chinese Academy of Sciences, Shanghai 200050, China

[§]Graduate School of Chinese Academy of Sciences, Beijing 100049, China

ABSTRACT: The ternary boron compounds $TM_7TM'_6B_8$ (TM = Ta, Nb; TM' = Ru, Rh, Ir) were prepared by high-temperature thermal treatment of mixtures of the elements. An analysis of the chemical bonding by the electron density/electron localizability approach reveals formation of covalently bonded polyanions $[B_6]$ and $[TM'_6B_2]$. The cationic part of the structure contains separated TM cations. In agreement with the chemical bonding analysis and band structure calculations, all $TM_7TM'_6B_8$ compounds are metallic Pauli-paramagnets (TM' = Ru, Rh) or diamagnets (TM' = Ir).

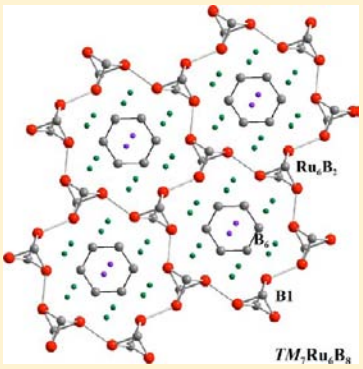

INTRODUCTION

Transition-metal borides are known for their physical, chemical, and mechanical properties, in particular, combining high hardness, refractory behavior, chemical inertness, and metallic conductivity.[1−9] Extending from binary to ternary borides results in a plethora of compounds with complex crystal structures.[10−14] These ternary phases can contain transition metals, as well as rare-earth metals. The structural complexity is caused in particular by the need of saturation of the valence requirements of the electron-deficient boron atoms.[15,16] Depending on the metal-to-boron ratio, one-, two- and three-dimensional arrangements of covalently bonded boron atoms are formed.[12,14,17,18] The wealth of observed physical properties comprises collective magnetism,[19−22] superconductivity,[23−26] interplay of magnetism with superconductivity,[27] thermoelectricity,[28−30] valence fluctuations,[31] Kondo lattice behavior,[32] heavy fermion behavior,[33] etc. To mention only a few of the well-known materials of high technological relevance there are $Nd_2Fe_{14}B$-based permanent magnets,[34] boride-containing metallic glasses,[35] and LaB_6-based electron emitters for electron microscopes.[36] Possible applications as refractory cermet materials have driven the study of ternary transition-metal-based borides for several decades.[3,37−43]

The systematic search for new phases has been also extended to systems containing platinum group metals[44−54] and gains additional crystal chemical insights with respect to the underlying chemical bonding situation as well as structure−property relationships.

In this study, we report on the synthesis, crystal structure, chemical bonding, and physical properties of new compounds $TM_7TM'_6B_8$ (TM = Ta, Nb; TM' = Ru, Rh, Ir). These six phases were discovered in the course of a systematic search for new materials with trigonal-prismatic coordination of boron atoms. First results on this study were reported at the international symposium on boron and boron compounds.[55]

EXPERIMENTAL SECTION

Preparation. The samples with nominal compositions $TM_3TM'_3B_4$ and $TM_7TM'_6B_8$ (TM = Nb, Ta; TM' = Ru, Rh, Ir) were synthesized by arc-melting the elements on a water-cooled copper hearth under argon. Foils of tantalum (Chempur, 99.9 mass %), niobium (Chempur, 99.9 mass %), rhodium (Chempur, 99.9 mass %), and iridium (Chempur, 99.9 mass %), as well as powders of ruthenium (Chempur, 99.9 mass %) and crystalline boron (Alfa Aesar, 99.999 mass %), were used as initial reagents. Ruthenium powder was first pressed into pellets. Boron powder and the TM' metal foils, ingots, or pellets were embedded in tantalum or niobium foils and arc-melted several times to obtain homogeneous samples. During the melting process, the weight losses were negligible (<0.1 mass %). The obtained ingots were put into ZrO_2 crucibles, sealed in Ta tubes, and then annealed at 1500−1650 °C in a high temperature furnace (HTM Reetz LORA) for 3 or 4 days under argon. All manipulations were performed inside an argon-filled MBraun glovebox (O_2/H_2O content ≤1 ppm). The as-cast and annealed samples are stable in air for a long time.

Received: September 8, 2011
Published: June 22, 2012

Table 1. Crystallographic Data for $TM_7TM'_6B_8$ (TM = Ta, Nb; TM' = Ru, Rh)

	$Nb_7Ru_6B_8$	$Ta_7Ru_6B_8$	$Nb_7Rh_6B_8$	$Ta_7Rh_6B_8$
space group	$P6/m$	$P6/m$	$P6_3/m$	$P6_3/m$
lattice parameters[a]				
a (Å)	9.5061(2)	9.4695(3)	16.1309(7)	16.0861(7)
c (Å)	3.1284(1)	3.1370(2)	6.5686(4)	6.5592(6)
V (Å^3)	244.83(3)	243.61(3)	1480.2(2)	1469.9(3)
ρ (g cm^{-3})	9.11(1)	13.36(1)	9.12(2)	13.36(1)
diffraction system	Rigaku R-Axis Rapid		Rigaku AFC7	
radiation, λ (Å)	0.71073		0.71073	
$2\theta_{max}$ (°)	120	120	67.03	67.42
$N(hkl)_{measured}$	6602	10794	13125	13925
$N(hkl)_{unique}$	1374	1367	2026	2013
$N(hkl)_{observed}$ ($F_{hkl} > 4\sigma(F)$[b])	1374	1367	817	792
R_{int}/R_σ	0.025/0.026	0.035/0.026	0.054/0.021	0.049/0.014
refined parameters	24	24	84	107
extinction coefficient	0.0084(4)	0.0098(2)	0.00016(2)	0.000228(9)
R_F/wR_F^2	0.036/0.039	0.038/0.041	0.026/0.051	0.027/0.040

[a]Powder XRD data for all compounds. [b]$F_{hkl} > 6\sigma(F)$ for $Ta_7Ru_6B_8$

Characterization. Powder X-ray diffraction (XRD) of the products was performed on a HUBER G670 imaging plate Guinier camera with Cu Kα_1 radiation (λ = 1.540598 Å). The *WinXpow* program package[56] was used to carry out the phase identification. Lattice parameters refinement by least-squares fitting (LaB_6 internal standard correction) and crystal structure solution and refinement have been done using the program package *WinCSD*.[57] Rietveld refinements on the multiphase samples were carried out using the software package *fullProf*.[58]

Single crystals of $Ta_7Ru_6B_8$, $Nb_7Ru_6B_8$, $Nb_7Rh_6B_8$, and $Ta_7Rh_6B_8$ were selected from annealed samples. Diffraction data were collected on a Rigaku R-Axis Rapid diffraction system or Rigaku AFC7 diffractometer equipped with a Mercury CCD detector (Mo Kα radiation, λ = 0.71073 Å). The crystal structures were solved by direct phase determination method and refined by a full-matrix least-squares procedure using the program package *WinCSD*.[57]

Metallography. Specimens of several-millimeters size were cut from the annealed samples for metallographic investigations. They were embedded in conductive resin and then submitted to multistep grinding and polishing processes with final polishing using 0.25-μm diamond powder. The microstructure was investigated on a light-optical microscope (Axioplan2, Zeiss) as well as a scanning electron microscope (Philips XL 30 with a LaB_6 cathode, S-UTW-Si-(Li) detector, FEI, standardless technique). Composition of the observed phases was analyzed by energy dispersive X-ray spectroscopy (EDXS, Philips XL 30) and wavelength dispersive X-ray spectroscopy (WDXS, Cameca SX 100, W cathode, S-UTW-Si-(Li) detector) using B Kα, Ta Lα, Ru Lα signals and elemental Ta, Nb, Ru, Rh, Ir, and Pd_3B or Ni_3B as standards.

Calculations Procedure. The electronic structure for all investigated compounds was computed with the TB-LMTO-ASA[59] program package using the experimental structure parameters. It was not necessary to add empty spheres. Basis sets containing Ta(6*s*, 6*p*, 5*d*), Nb(5*s*, 5*p*, 4*d*), Ru(5*s*, 5*p*, 4*d*), Rh(5*s*, 5*p*, 4*d*), and B(2*s*, 2*p*) orbitals were used for self-consistent calculations with Ta(5*f*), Nb(4*f*), Rh(4*f*), Ru(4*f*), and B(3*d*) functions being downfolded. The following radii of the atomic spheres were applied for the calculations: r(Nb1) = 1.720 Å, r(Nb2) = 1.639 Å, r(Ru) = 1.402 Å, r(B1) = 1.156 Å, r(B2) = 1.069 Å for $Nb_7Ru_6B_8$; r(Nb) = 1.565 Å − 1.795 Å, r(Rh) = 1.339 Å − 1.479 Å, r(B1) = 1.074 Å − 1.109 Å, for $Nb_7Rh_6B_8$, and r(Ta1) = 1.722 Å, r(Ta2) = 1.634 Å, r(Ru) = 1.400 Å, r(B1) = 1.155 Å, r(B2) = 1.069 Å for $Ta_7Ru_6B_8$. For the analysis of the chemical bonding, the electron density and the electron localizability indicator (ELI-D, Y_D)[60,61] were calculated on an equidistant grid (mesh around 5 pm) with a dedicated module implemented in the TB-LMTO-ASA program.

The electron density and ELI-D distributions were further processed by the program DGrid[62] to study their topology, determine the respective basins as well as their electron populations. Basins[63] are non-overlapping space-filling regions of space, each enclosing a maximum (attractor) of the examined field. The basins are bounded by surfaces of zero-flux of the corresponding gradient field. Summing up the electron populations of all basins found in a unit cell yields the total number of electrons in the unit cell.

Physical Properties. Temperature-dependent magnetization data of samples of the $TM_7TM'_6B_8$ compounds were measured in a SQUID magnetometer (MPMS XL-7, Quantum Design) at fields μ_0H from 2 mT to 7 T in the temperature range 1.8−400 K. Diamagnetic signals below 5 K indicated superconducting transitions of secondary phases in some samples in 2 mT field (less than 7% of full shielding, i.e., of $-1/4\pi$, and <2% Meissner effect). The electrical resistivity of the $Ta_7Ru_6B_8$ sample was measured by the dc four-point method between 4 and 320 K.

RESULTS AND DISCUSSION

Crystal Structure Determination. *$Nb_7Ru_6B_8$ and $Ta_7Ru_6B_8$.* The powder XRD pattern of a sample with nominal composition $Ta_3Ru_3B_4$ could not be assigned to any known binary or ternary compounds in the Ta−Ru−B system.[64] The WDXS analysis revealed the presence of an unknown phase with the composition $Ta_{30.7(2)}Ru_{29.7(2)}B_{39.7(4)}$. The 39 strongest reflections of the powder XRD pattern were indexed successfully in a hexagonal unit cell with lattice parameters a = 9.4695(3) Å, c = 3.1390(2) Å using the automatic indexing algorithm TREOR within the *WinXPow* program package.[56] Analysis of the extinction conditions indicated the primitive Bravais group. The space group $P6/m$ was chosen for the structure determination. In the first step, heavy Ta and Ru atoms were localized by direct phase determination procedure, and boron positions were obtained from the difference Fourier maps (*WinCSD* program package[57]). The refined composition $Ta_7Ru_6B_8$ ($Ta_{33.3}Ru_{28.6}B_{38.1}$) agrees well with the one obtained from WDXS. Low residuals (R_I = 0.045, R_P = 0.102) indicated reliability of the obtained model. However, the displacement parameters of the boron atoms could not be refined satisfactorily from powder XRD data; thus, a single crystal diffraction experiment was performed.

Crystallographic details on the single crystal data collection for the borides $Nb_7Ru_6B_8$ and $Ta_7Ru_6B_8$ are listed in Table 1. As a starting model for the refinement, the crystal structure of $Ta_7Ru_6B_8$ obtained from powder methods was used. Final atomic coordinates and anisotropic displacement parameters are presented in Table 2, and the shortest interatomic distances as well as a coordination numbers of atoms are collected in Table 3.

dx.doi.org/10.1021/ic201978n | *Inorg. Chem.* 2012, 51, 7472−7483

Table 2. Atomic Coordinates and Anisotropic Displacement Parameters for $TM_7Ru_6B_8$[a] and $TM_7Rh_6B_8$[b,c,d]

atom	site	x/a	y/b	z/c	B_{iso}/B_{eq}	B_{11}	B_{22}	B_{33}	B_{12}
$Nb_7Ru_6B_8$									
Nb1	1*a*	0	0	0	0.254(6)	0.223(7)	B_{11}	0.24(1)	$B_{11}/2$
Nb2	6*j*	0.08627(3)	0.36335(3)	0	0.328(4)	0.252(5)	0.442(5)	0.275(5)	0.161(4)
Ru	6*k*	0.51373(2)	0.15405(2)	1/2	0.283(4)	0.242(4)	0.242(4)	0.366(4)	0.102(3)
B1	2*c*	1/3	2/3	0	0.46(6)	0.37(7)	B_{11}	0.5(1)	$B_{11}/2$
B2	6*k*	0.2210(3)	0.0661(3)	1/2	0.29(5)	0.26(5)	0.28(5)	0.41(5)	0.19(5)
$Ta_7Ru_6B_8$									
Ta1	1*a*	0	0	0	0.128(3)	0.150(4)	B_{11}	0.045(5)	$B_{11}/2$
Ta2	6*j*	0.08648(2)	0.36398(2)	0	0.192(3)	0.187(3)	0.263(3)	0.118(2)	0.106(2)
Ru	6*k*	0.51327(3)	0.15406(3)	1/2	0.170(4)	0.142(5)	0.155(5)	0.207(4)	0.071(4)
B1	2*c*	1/3	2/3	0	0.52(8)	0.4(1)	B_{11}	0.6(1)	$B_{11}/2$
B2[e]	6*k*	0.2221(5)	0.0662(4)	1/2	0.29(7)	0.68(9)	0.09(7)	0.24(6)	0.27(7)
$Nb_7Rh_6B_8$									
Nb1	2*c*	1/3	2/3	1/4	0.44(3)	0.40(4)	B_{11}	0.41(6)	$B_{11}/2$
Nb2	2*d*	2/3	1/3	1/4	0.44(3)	0.39(4)	B_{11}	0.45(6)	$B_{11}/2$
Nb3	2*b*	0	0	1/4	0.41(4)	0.45(5)	B_{11}	0.30(8)	$B_{11}/2$
Nb4	6*h*	0.0737(1)	0.2184(1)	1/4	0.33(4)	0.39(4)	0.42(4)	0.45(4)	0.24(4)
Nb5	6*h*	0.5525(1)	0.8184(1)	1/4	0.49(4)	0.41(4)	0.55(4)	0.42(4)	0.16(4)
Nb6	6*h*	0.2117(1)	0.1529(1)	1/4	0.46(4)	0.66(5)	0.54(4)	0.36(4)	0.35(4)
Nb7	6*h*	0.4506(1)	0.1831(1)	1/4	0.40(3)	0.36(4)	0.36(4)	0.48(4)	0.15(4)
Nb8	6*h*	0.6025(1)	0.1234(1)	1/4	0.58(4)	0.53(5)	0.55(4)	0.42(4)	0.22(4)
Nb9	6*h*	0.3993(1)	0.8784(1)	1/4	0.50(4)	0.54(5)	0.49(4)	0.46(4)	0.31(4)
Rh1	12*i*	0.44354(6)	0.04172(7)	0.5263(2)	0.52(2)	0.45(3)	0.47(3)	0.71(3)	0.22(2)
Rh2	12*i*	0.29273(7)	0.06917(7)	0.4914(1)	0.56(3)	0.53(3)	0.50(3)	0.53(3)	0.27(2)
Rh3	12*i*	0.37514(6)	0.26456(6)	0.4682(2)	0.39(2)	0.52(3)	0.45(3)	0.27(2)	0.24(2)
B1	6*h*	0.332(1)	0.998(1)	1/4	0.5(1)				
B2	6*h*	0.313(1)	0.330(1)	1/4	0.5(1)				
B3	12*i*	0.5453(9)	0.3063(9)	0.494(2)	0.5(1)				
B4	12*i*	0.5663(9)	0.2033(9)	0.512(2)	0.5(1)				
B5	12*i*	0.0984(9)	0.1274(9)	0.496(2)	0.5(1)				
$Ta_7Rh_6B_8$									
Ta1	2*c*	1/3	2/3	1/4	0.35(2)	0.28(3)	B_{11}	0.39(4)	$B_{11}/2$
Ta2	2*d*	2/3	1/3	1/4	0.32(2)	0.22(3)	B_{11}	0.39(4)	$B_{11}/2$
Ta3	2*b*	0	0	1/4	0.41(3)	0.30(3)	B_{11}	0.49(6)	$B_{11}/2$
Ta4	6*h*	0.44966(7)	0.26458(7)	1/4	0.65(3)	0.67(3)	0.73(3)	0.55(3)	0.35(3)
Ta5	6*h*	0.15224(7)	0.21318(7)	1/4	0.57(3)	0.47(3)	0.59(3)	0.62(3)	0.25(3)
Ta6	6*h*	0.51730(7)	0.11953(7)	1/4	0.55(3)	0.50(3)	0.62(3)	0.47(3)	0.25(3)
Ta7	6*h*	0.21825(7)	0.07149(7)	1/4	0.47(3)	0.48(3)	0.54(3)	0.51(3)	0.34(3)
Ta8	6*h*	0.54518(7)	0.72949(7)	1/4	0.51(3)	0.54(3)	0.63(3)	0.43(3)	0.35(3)
Ta9	6*h*	0.48060(7)	0.88042(7)	1/4	0.65(3)	0.72(3)	0.71(3)	0.64(3)	0.43(3)
Rh1	12*i*	0.0687(1)	0.29161(9)	0.4681(2)	0.35(3)	0.38(4)	0.39(4)	0.33(4)	0.22(3)
Rh21[f]	12*i*	0.5972(2)	0.0418(2)	0.4796(4)	0.36(6)	0.34(8)	0.38(8)	0.37(8)	0.18(7)
Rh22[f]	12*i*	0.5973(2)	0.0412(2)	0.5175(4)	0.40(6)	0.36(8)	0.42(8)	0.43(8)	0.20(7)
Rh31[f]	12*i*	0.3738(2)	0.1095(2)	0.4869(4)	0.41(7)	0.41(8)	0.38(8)	0.44(8)	0.19(7)
Rh32[f]	12*i*	0.3746(2)	0.1102(2)	0.5259(4)	0.36(6)	0.38(8)	0.34(8)	0.36(8)	0.18(6)
B1	6*h*	0.684(2)	0.020(2)	1/4	0.8(4)				
B2	6*h*	0.335(2)	0.001(2)	1/4	0.6(4)				
B3	12*i*	0.540(2)	0.243(2)	0.505(3)	0.6(3)				
B4	12*i*	0.125(2)	0.101(2)	0.495(3)	0.7(3)				
B5	12*i*	0.638(2)	0.205(2)	0.489(3)	0.7(3)				

[a] $B_{13} = B_{23} = 0$ for $Nb_7Rh_6B_8$ and $Ta_7Rh_6B_8$. [b] Anisotropic displacement parameters for boron atoms were not refined for $Nb_7Rh_6B_8$ and $Ta_7Rh_6B_8$. [c] $B_{13} = B_{23} = 0$ for Nb1–Nb9; $B_{13} = -0.00(2)$, $B_{23} = -0.01(2)$ for Rh1; $B_{13} = -0.01(2)$, $B_{23} = -0.05(2)$ for Rh2; $B_{13} = 0.02(2)$, $B_{23} = -0.04(2)$ for Rh3. [d] $B_{13} = B_{23} = 0$ for Ta1–Ta9; $B_{13} = -0.03(3)$, $B_{23} = -0.03(3)$ for Rh1; $B_{13} = 0.01(6)$, $B_{23} = 0.06(6)$ for Rh21; $B_{13} = 0.00(6)$, $B_{23} = 0.00(6)$ for Rh22; $B_{13} = -0.01(6)$, $B_{23} = 0.01(6)$ for Rh31, $B_{13} = 0.01(6)$, $B_{23} = 0.01(6)$ for Rh32. [e] The strong anisotropy of displacement for B2 is probably caused by the correlations in refinement in presence of the strong scatters like Ta. [f] Occupancy for the positions Rh21, Rh22, Rh31, and Rh32 was fixed to 0.5.

$Nb_7Rh_6B_8$ and $Ta_7Rh_6B_8$. The reflections of the impurity phases *TM*B and *TM*Rh_3 always appeared in XRD powder patterns of the $TM_7Rh_6B_8$ samples (Figure 1). Nevertheless, the crystal structures of $Nb_7Rh_6B_8$ and $Ta_7Rh_6B_8$ were refined first from the powder diffraction data using the atomic coordinates of the according ruthenium compounds. The refinements yielded relatively low residuals ($R_B = 0.053$ and 0.044, $R_P = 0.047$ and 0.042 for $Nb_7Rh_6B_8$ and $Ta_7Rh_6B_8$, respectively) but run quite

dx.doi.org/10.1021/ic201978n | Inorg. Chem. 2012, 51, 7472–7483

Table 3. Interatomic Distances (Å) in the Structures of $TM_7TM'_6B_8$

atoms		$Nb_7Ru_6B_8$	$Ta_7Ru_6B_8$	$Nb_7Rh_6B_8$	$Ta_7Rh_6B_8$	CN[a]
*TM*1 or Nb1–Nb3	−12B2	2.436(2)	2.441(3)	2.45(3)–2.50(4)	2.43(2)–2.54(2)	20
	−6*TM*2	3.1257(3)	3.1189(2)	3.003(4)–3.138(4)	3.031(1)–3.100(1)	
	−2*TM*2	3.1284(3)	3.1370(3)	3.2843(2)	3.2796(2)	
*TM*2 or Nb4–Nb9	−2B2	2.364(2)	2.362(3)	2.29(3)–2.41(3)	2.29(2)–2.41(2)	16
	−2B2	2.366(2)	2.363(3)	2.38(2)–2.47(4)	2.35(2)–2.48(2)	
	−1B1	2.6567(3)	2.6420(2)	2.48(2)–2.96(2)	2.35(3)–2.90(3)	
	−2*TM*′	2.7441(3)	2.7346(3)	2.621(4)–2.798(4)	2.662(3)–2.902(3)	
	−2*TM*′	2.7544(3)	2.7472(3)	2.751(4)–2.924(4)	2.658(3)–2.914(3)	
	−2*TM*′	2.8457(3)	2.8396(3)	2.798(4)–2.973(4)	2.672(2)–2.937(2)	
	−1*TM*1	3.1257(3)	3.1189(2)	3.003(4)–3.138(4)	3.031(1)–3.100(1)	
	−2*TM*2	3.1257(4)	3.1189(2)	2.894(5)–3.252(5)	2.957(2)–3.201(2)	
	−2*TM*2	3.1284(1)	3.1370(2)	3.2845(2)–3.2913(4)	3.2798(2)–3.2829(2)	
TM′ or Rh1–Rh3	−2B1	2.2333(2)	2.2330(3)	2.11(1)–2.40(2)	2.13(2)–2.50(2)	12
	−1B2	2.473(3)	2.450(4)	2.36(3)–2.48(3)	2.36(2)–2.46(2)	
	−2*TM*′	2.7608(3)	2.7529(4)	2.696(4)–2.713(4)	2.677(3)–2.705(4)	
	−1*TM*′	2.8073(3)	2.8005(4)	2.746(4)–2.772(3)	2.704(4)–2.753(3)	
	−2*TM*2	2.7441(3)	2.7346(3)	2.621(4)–2.751(4)	2.658(3)–2.720(3)	
	−2*TM*2	2.7544(3)	2.7472(3)	2.745(4)–2.873(3)	2.734(3)–2.831(3)	
	−2*TM*2	2.8457(3)	2.8396(3)	2.809(4)–2.973(4)	2.838(3)–2.937(2)	
B1 or B1–B2	−6*TM*′	2.2333(2)	2.2330(3)	2.11(1)–2.39(1)	2.13(2)–2.50(2)	9
	−3*TM*2	2.6567(3)	2.6420(2)	2.38(2)–2.96(2)	2.35(3)–2.90(3)	
B2 or B3–B5	−2B2	1.868(4)	1.870(6)	1.84(4)–1.87(6)	1.74(3)–1.96(3)	9
	−2*TM*2	2.364(2)	2.362(3)	2.29(3)–2.41(3)	2.29(2)–2.39(2)	
	−2*TM*2	2.366(2)	2.363(3)	2.42(3)–2.49(3)	2.39(2)–2.48(2)	
	−2*TM*1	2.436(2)	2.441(3)	2.39(3)–2.57(3)	2.43(2)–2.54(2)	
	−1*TM*′	2.473(3)	2.450(4)	2.36(3)–2.48(3)	2.36(2)–2.46(2)	

[a]CN = coordination number.

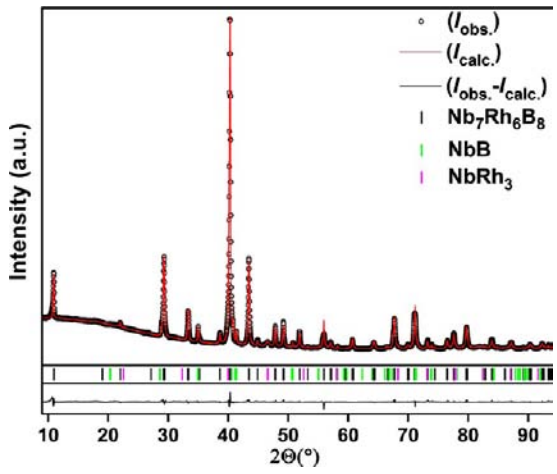

Figure 1. Powder XRD pattern of the sample $Nb_7Rh_6B_8$.

instable, so that the displacement parameters of the boron atoms had to be fixed. The obtained solutions were characterized by rather short B–B distances within the B_6 ring (1.56 Å and 1.63 Å for $Nb_7Rh_6B_8$ and $Ta_7Rh_6B_8$, respectively). Interestingly, another solution showing very similar residual values was found for $Nb_7Rh_6B_8$, but the B–B distances in the B_6 ring were close to 1.8 Å and unusual displacement parameters resulted for the metal atoms. Constructive suggestions of one of the reviewers prompted our further attempts to prepare single crystals of $Nb_7Rh_6B_8$ and $Ta_7Rh_6B_8$. Both compounds form either by solid-state reactions (peritectoid) or by peritectic reaction with very narrow liquidus surface. Thus, after several attempts, only small single-crystalline fragments were separated from the samples with stoichiometric compositions. The strong reflections of the single crystal diffraction data for the $TM_7Rh_6B_8$ compounds were indexed with hexagonal unit cells analogous to the ruthenium compounds. The refinement of the crystal structure of $Nb_7Rh_6B_8$ with this unit cell resulted in a low residual value $R_F = 0.022$ (for 344 reflections and 31 refined parameters), and revealed that the Rh atoms are no longer located on the mirror planes and that the B1 atoms show extreme anisotropy of the displacement in the (001) plane. Both facts suggested the presence of a superstructure. Indeed, a more detailed analysis of the diffraction data highlighted additional reflections which were described in a larger unit cell with $a = a(Nb_7Ru_6B_8)\sqrt{3}$ and $c = 2c(Nb_7Ru_6B_8)$. Analysis of the systematic extinctions suggested the possible space groups $P6_3/m$ and $P6_3$. The crystal structure of $Nb_7Rh_6B_8$ was solved and refined in the centrosymmetric space group. It is worth mentioning that, caused by the small number and relatively low intensity superstructure reflections, the refinement was not running straightforward. Thus, a special treatment of the strongly correlated parameters was necessary, leading to a final residual of $R_F = 0.026$ for 817 reflections and 84 refined parameters. Crystallographic data of $Nb_7Rh_6B_8$ are listed in Table 1, final atomic coordinates and displacement parameters are collected in Table 2. Interatomic distances are presented in Table 3.

The diffraction experiment on the single-crystalline specimen of $Ta_7Rh_6B_8$ revealed the presence of a superstructure analogous to the niobium–rhodium compound with the lattice parameters $a = 16.0861(7)$ Å and $c = 6.5592(6)$ Å. A refinement of the crystal structure with the model of $Nb_7Rh_6B_8$ led to low residual values but extremely strong anisotropy in atomic displacement for the Rh2 and Rh3 positions with $B_{11} \approx B_{22} \ll B_{33}$, suggesting a crystallographic disorder along the [001] direction. In the final refinement, the electron density in these parts of the crystal

dx.doi.org/10.1021/ic201978n | Inorg. Chem. 2012, 51, 7472–7483

structure was described with equally occupied split positions and the values of the z coordinate approximately symmetrical with respect to $z = 0.5$. As for $Nb_7Rh_6B_8$, a special treatment of the strongly correlated parameters was necessary for $Ta_7Rh_6B_8$, leading to a final residual of $R_F = 0.027$ for 792 reflections and 107 refined parameters. Crystallographic data of $Ta_7Rh_6B_8$ are listed in Table 1, final atomic coordinates and displacement parameters are collected in Table 2, interatomic distances are presented in Table 3.

$Nb_7Ir_6B_8$ and $Ta_7Ir_6B_8$. The compounds $Ta_7Ir_6B_8$ and $Nb_7Ir_6B_8$ were observed only in multiphase samples. Therefore, we report here only subcell unit cell parameters $a = 9.2885(4)$ Å, $c = 3.3164(3)$ Å and $a = 9.3178(7)$ Å, $c = 3.3192(5)$ Å, respectively. Taking in account the chemical analogy of Rh and Ir in intermetallic compounds, a formation of the superstructure such as in the rhodium compounds is very probable. Nevertheless a proof of the superstructure using the powder diffraction data failed, due to the very low relative intensity of the superstructure reflections.

Crystal Chemistry. In the crystal structures of $TM_7Ru_6B_8$ and $TM_7Rh_6B_8$, the *TM* atoms reside in two kinds of environments. The first one is a 20-vertices polyhedron consisting of 12 B and 8 *TM* atoms (Figure 2a). Such polyhedra are observed also for Al atoms in AlB_2 and are characteristic for binary compounds NbB_2, TaB_2 (structure type AlB_2), Nb_3B_4 (structure type Ta_3B_4[65]), and Nb_5B_6 (structure type V_5B_6[66]). The second kind of coordination sphere for TM atoms is an 16-vertices polyhedron, which is similar to that of *TM*1 and is often observed for transition-metal atoms in the ternary compounds of main-group elements (e.g. gallium) with transition metals and more electropositive components (alkaline-earth, rare-earth metals).[67] The Ru and Rh atoms reside in a distorted cuboctahedron, which is a common building unit in many transition-metal borides, in particular in the series of derivatives of the $CaCu_5$ type.[12] Finally, B atoms center tricapped trigonal prisms formed either by 6 *TM*′ and 3 *TM* atoms or by 6 *TM*, 1 *TM*′, and 2 B atoms. The trigonal-prismatic coordination of boron is also a common feature of all the mentioned borides (Figure 2a). The spatial arrangement of the latter prisms in form of hexagonal columns along [001] brings the centering boron atoms in close contact, thus resulting in the formation of B_6 rings.

A comparison of the crystal structures of $TM_7Ru_6B_8$ and $TM_7Rh_6B_8$ revealed that the atomic arrangements within the trigonal prisms $[BTM_6]$ do not change markedly from Ru to Rh compounds (Figure 2 b,c). The main changes are observed within the $[BTM'_6]$ prisms, where the boron atoms are no longer located in the center and shifted toward one of the Rh pairs showing strongly reduced distances of 2.23 Å for the B1 position and 2.11 Å for the B2 position, respectively, and markedly increased distances to the two other pairs of the Rh atoms of 2.40 Å for the B1 position and 2.23 and 2.28 Å for the B2 position, respectively. For comparison, the corresponding Ru−B distances in the ruthenium compounds are all equal 2.23 Å (Table 3). The stronger B−Rh interactions for a part of Rh atoms lead to a puckering of the atomic layer containing only the transition metal atoms. This puckering gives rise to the increase of the translations in the (001) plane ($a = a(Nb_7Ru_6B_8)\sqrt{3}$) and doubling of the lattice parameter c (Figure 2d). While in the crystal structure of $Nb_7Rh_6B_8$ the puckered layers are arranged orderly along the direction [001], in the structure of $Ta_7Rh_6B_8$, they are disordered, which is visualized in the superstructure cell as splitting of the Rh2 and Rh3 sites.

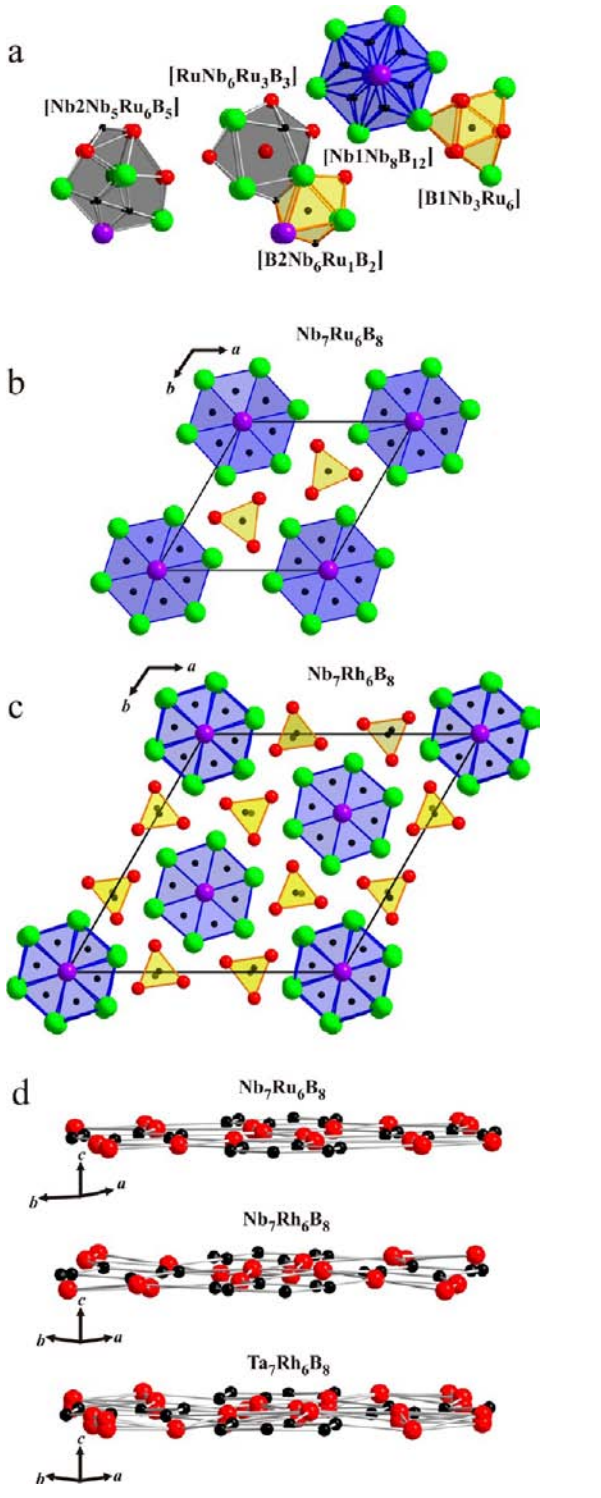

Figure 2. Crystal structures of $TM_7Ru_6B_8$ and $TM_7Rh_6B_8$: (a) coordination polyhedra of the *TM*, *TM*′, and boron atoms; (b, c) packings of the trigonal prisms around the boron atoms (blue, $[BTM_6]$; yellow, $[BTM'_6]$); (d) B−*TM*′ layers in the crystal structures of $Nb_7Ru_6B_8$, $Nb_7Rh_6B_8$, and $Ta_7Rh_6B_8$ showing the evolution of puckering ($Nb_7Rh_6B_8$) and disorder ($Ta_7Rh_6B_8$).

The crystal structures of the $TM_7TM'_6B_8$ compounds belong to the large group of the derivatives of the AlB_2 structure type.[68] The AlB_2 type can be presented as a packing of condensed $[BAl_6]$ trigonal prisms, completely filling the space. The crystal structure of U_2RuSi_3[69] adopts a superstructure of the AlB_2 type with

dx.doi.org/10.1021/ic201978n | Inorg. Chem. 2012, 51, 7472−7483

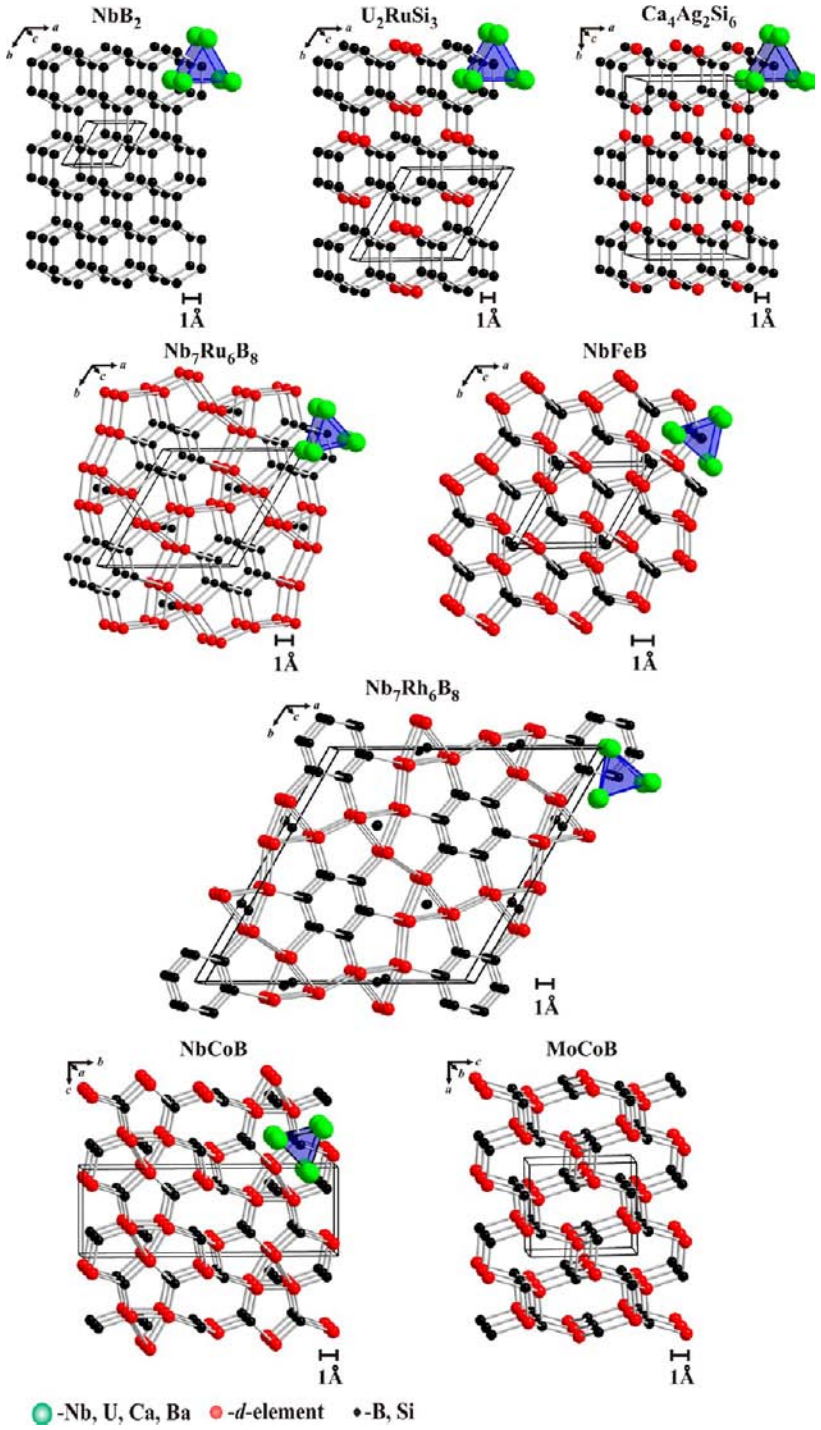

Figure 3. Boron−*TM*′ networks in some derivatives of the AlB_2 structure type.

doubled lattice parameters *a* and *b*. In this type, six in-plane condensed [SiU_6] trigonal prisms form columns sharing common faces along [001]. The trigonal-prismatic channels between the columns are filled by Ru atoms. The crystal structure of $Ca_4Ag_2Si_6$[70] shows a similar packing of prisms. In the structure of $Nb_7Ru_6B_8$, columns of six-condensed face-sharing [BNb_6] trigonal prisms, extend along [001]. Between the so formed columns, there is enough space for tricapped [$B1Nb_3Ru_6$] trigonal prisms and empty octahedra [$\square Ru_4Nb_2$]. In a more general way, the structural motifs of this kind may be described as a two-dimensional intergrowth of the AlB_2 (filled trigonal prisms) and α-Fe (empty (half)-octahedra) motifs with a general formula $(R, R')_{m+n}X_{2m}$ ($m = 4$, $n = 9$ for $TM_7TM'_6B_8$, Figure 2d).[71] A binary representative of the $TM_7TM'_6B_8$ structure should have a composition $R_{13}X_7$ and was not known until now. Three possible sites of the *R* component may be occupied by two different kinds of atoms: $R_7R'_6X_8$. The first occupation variant was found in $RE_7In_6Ni_{5\pm x}Ge_{3\pm x}$ (*RE* = Ce, Pr), *R* = *RE*, *R*′ = In, *X* = Ni, Ge.[72] The crystal structure of $TM_7TM'_6B_8$ is a chemical antitype to the $RE_7In_6(Ni,Ge)_8$ one, where the transition metal *TM*′ occupies the position of the main-group element In, and boron takes the places of the transition metal Ni (and Ge). Such a chemical homology is often observed in the triel compounds with trigonal prismatic coordination of atoms: RE_2GaNi_2 and

dx.doi.org/10.1021/ic201978n | *Inorg. Chem.* 2012, 51, 7472−7483

Mo_2NiB_2,[73] RE_3GaCo_3 and W_3CoB_3.[74] However, among the borides, the $R_{13}X_7$ structural pattern is found for the first time.

Interatomic distances in the crystal structures of $TM_7TM'_6B_8$ compounds are listed in Table 3. All of them are close or slightly larger than the sum of atomic radii of the elements ($r_{Nb} = r_{Ta}$ = 1.43 Å; $r_{Ru} = r_{Rh}$ = 1.34 Å; r_B = 0.83 Å).[75] *TM*−*TM* contacts in the (001) plane for $Nb_7Ru_6B_8$ and $Ta_7Ru_6B_8$ (3.1257(3) Å and 3.1189(2) Å, respectively) are both longer than *TM*−*TM* distances in the (001) plane in diborides (AlB_2 type of crystal structure) TMB_2 (3.1115 Å and 3.076 Å for NbB_2,[76] and TaB_2,[77] respectively). On the other hand, the *TM*−*TM* distances in the (001) plane vary between 3.003 Å and 3.138 Å for $Nb_7Rh_6B_8$ and between 3.031 Å and 3.100 Å for $Ta_7Rh_6B_8$, and are sometimes shorter than these in respective TMB_2. Comparing to $TM_7Rh_6B_8$, the structures of $TM_7Ru_6B_8$ are compressed along the [001] direction and enlarged in the (001) plane, which results in longer *TM*−*TM* distances in the (001) plane. The B−B distances building the hexagonal nets in TMB_2 are 1.796 Å and 1.776(6) Å in NbB_2 and TaB_2, respectively. The comparable B2−B2 distances in the isolated hexagonal rings in $TM_7TM'_6B_8$ are 1.868(4) Å, 1.870(6) Å, 1.84(4)−1.87(7) Å, and 1.74−1.96 Å in $Nb_7Ru_6B_8$, $Ta_7Ru_6B_8$, $Nb_7Rh_6B_8$, and $Ta_7Rh_6B_8$, respectively (Table 3). In $TM_7Rh_6B_8$ compounds, they seem to alternate slightly not being constrained by symmetry, but this is rather an effect of the refinement of a structure with high pseudosymmetry. Thus, the formation of (nearly) equidistant B_6 rings is a common feature of the $TM_7Ru_6B_8$ and $TM_7Rh_6B_8$ compounds despite the difference in the symmetry between their crystal structures.

On the base of analysis of interatomic distances, all structure types discussed above can be presented as consisting of atomic nets composed of six-member rings formed by boron and the more electronegative transition metal atom *TM*′ (Figure 3). The cations are embedded in the cavities formed by anionic nets. In NbB_2 boron atoms form in-plane condensed hexagonal rings. In the structure of U_2RuSi_3 the Si_6 rings are interconnected by Ru atoms. The same kind of network occurs in the compound $Ca_4Ag_2Si_6$ where the Si_6 units are interlinked by Ag atoms, the difference to U_2RuSi_3 is in the stacking manner of the rings. While in the three structures above anionic nets are planar, in the $TM_7TM'_6B_8$ compounds the electronegative atoms are organized in different levels. The B_6 rings are enveloped by coplanar condensed TM'_{12} rings, which are interconnected along the [001] direction by B atoms six-coordinated by *TM*′. Special attention should be paid to the distances between the B_6 ring and neighboring *TM*′ atoms. In case of the ruthenium compound they are in the region of 2.45−2.47 Å, while for the rhodium representative they vary from 2.36 to 2.48 Å. Localization of more electronegative atoms in two levels is common for the $TM_7TM'_6B_8$ and equiatomic compounds *TMTM*′B. In NbFeB (ZrNiAl type)[78] the interconnection of layers along [001] is realized by boron atoms, as in $TM_7TM'_6B_8$. However, within the plane nets, instead of the B_6 rings, only single boron atoms are present. In NbCoB[79] (prototype structure), the *TM*′-B network possesses more three-dimensional character, whereby the interconnection by six-coordinated boron atoms is still available together with a new interconnection pattern formed by four-coordinated B atoms. Finally, in MoCoB (TiNiSi-type),[80] only four-coordinated B atoms form a 3D framework together with four-coordinated *TM*′ atoms (Figure 3).

The rather short interatomic distances within the B_6 rings and between the ring atoms and the neighboring *TM*′ atoms raise the question, how far the network representation (Figure 3) is in accordance with the chemical bonding situation in the $TM_7TM'_6B_8$ compounds. In order to shed more light on atomic interactions, we analyzed them applying quantum-chemical calculations.

Electronic Structure and Chemical Bonding. *Electronic Density of States.* The electronic density of states (DOS) for $Nb_7Ru_6B_8$ (Figure 4, top) exhibits a pseudogap at around 0.3 eV

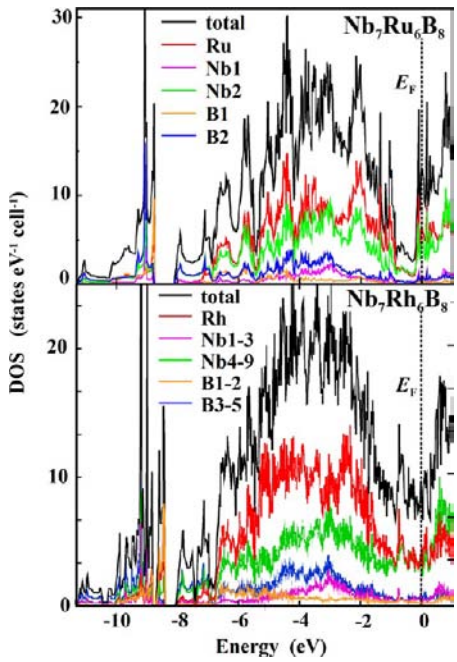

Figure 4. Electronic DOS for $Nb_7Ru_6B_8$ (top) and $Nb_7Rh_6B_8$ (bottom). DOS values are given for the unit cell with 21 atoms.

below the Fermi level, where the DOS drops to roughly 2 states/eV and cell. Additionally, there is a separate region below −8.5 eV with two DOS peaks. A closer inspection shows that the peak at lower energy (−9.1 eV) is due to states of B2 (i.e., the B_6 ring) mixed with the Nb states. The second peak (−8.8 eV) is mainly due to the mixing of the B1 with the Ru states.

The substitution of Ru with Rh reduces the pseudogap, electronic DOS increases in this region from 2 to 7 states/eV unit cell (normalized for the $Nb_7Ru_6B_8$-like subcell, Figure 4, bottom). There is again a separate region at low energies. Due to small changes in the crystal structure, each of two pronounced DOS peaks observed in $Nb_7Ru_6B_8$ splits in a group in $Nb_7Rh_6B_8$. The mixing of the B1, B2 (which are equivalent to B1 in $Nb_7Ru_6B_8$) and Rh states occurs between −8.5 and −9 eV; the region at E < 9 eV is mainly formed by the states of B3−B5 (structurally equivalent to B2 in $Nb_7Ru_6B_8$) and Nb.

Electronic Density. In the quantum theory of atoms in molecules (QTAIM) of Bader[63] the electron density basins usually represent the individual atoms in the system (i.e., when a nucleus is centered in the basin; however, the occurrence of so-called non-nuclear attractors for the electron density is also possible[81]). The difference between the electron population of the basin surrounding the nucleus and the nuclear charge yields the charge of the atomic basin, which is often relatively close to the formal charge of the examined atomic species. For the compounds $Nb_7Ru_6B_8$ and $Ta_7Ru_6B_8$, the atomic basins were determined and the corresponding atomic volumes and charges computed. They are exemplary presented for $Nb_7Ru_6B_8$ in Figure 5. The atomic basin for Nb1 is almost spherical, whereas the Ru basins are bounded by more or less plane surfaces. The Ru basins

dx.doi.org/10.1021/ic201978n | Inorg. Chem. 2012, 51, 7472−7483

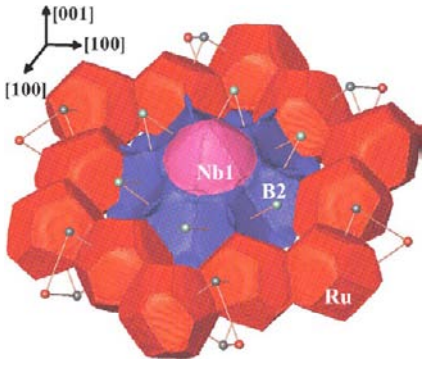

Figure 5. QTAIM atoms in $Nb_7Ru_6B_8$. Basins for Nb1 (magenta), Ru (red), and B2 (blue) are shown. The black, red and green spheres represent the B1, Ru, and Nb2 atoms, respectively.

form a ring around the B_6 basins. The atomic volumes, compiled in Table 4, reveal that for a given site the volumes vary only in the range of about 3% for both examined $TM_7Ru_6B_8$ compounds.

Table 4. Atomic Volumes (Å^3) and Charges for $Nb_7Ru_6B_8$ and $Ta_7Ru_6B_8$

	atomic volumes		atomic charges	
atoms	$Nb_7Ru_6B_8$	$Ta_7Ru_6B_8$	$Nb_7Ru_6B_8$	$Ta_7Ru_6B_8$
*TM*1	11.17	11.21	+1.64	+1.81
*TM*2	12.68	12.86	+1.09	+1.11
TM′	15.30	15.04	−0.68	−0.68
B1	7.19	7.09	−0.19	−0.18
B2	8.56	8.46	−0.65	−0.67

A similar trend is found for the atomic charges (Table 4), with the largest variance for the *TM1* atom at the 1*a* site. The transition metals Nb and Ta exhibit positive atomic charges of around +1.7 and +1.1 (*TM*1 and *TM*2) at 1*a* and 6*j* sites, respectively. The more electronegative transition metals *TM*′ (i.e. Ru) are negatively charged (−0.68) with charges comparable to the ones of the B2 atoms (−0.65 or −0.67), whereas the negative charges of the basins for the B1 atoms are close to zero. Actually, the B2 charges are not significantly different from the atomic charge of the boron atom (−0.57) in NbB_2 (based on TB-LMTO-ASA calculations employing data of reference[82]) and in MgB_2 (−0.7).[83] From the viewpoint of QTAIM volumes and charges, there is no evident change in the overall situation when comparing the examined $TM_7Ru_6B_8$ compounds.

Electron Density−Electron Localizability Approach. Further analysis of the chemical bonding in $TM_7TM'_6B_8$ compounds was performed applying electron density-electron localizability approach in real space[84] and using electron localizability indicator[60] in its ELI-D representation as bonding descriptor.[61] Because ELI-D reveals regions of space that can be used as descriptors of atomic shells, bonds, and lone-pairs, respectively, the examination of ELI-D may shed more light on the changes in the electronic structure accompanying the substitution of the *TM* and *TM*′ atoms. ELI-D describes the correlation of electronic motion. It is proportional to the electron population needed to form a fixed fraction of an electron pair. High ELI-D values describe regions were an electron is "alone". In analogy to the QTAIM approach ELI-D basins can be determined and assigned to chemically meaningful descriptors.

Bonding in B_6 Ring. The 1.286- and 1.300-localization domains (isosurfaces for the given isovalue) of Y_D^α (ELI-D based on $\alpha\alpha$-spin electron pairs) in Figure 6 show the bonding situation for the B_6 ring in $Nb_7Ru_6B_8$, $Ta_7Ru_6B_8$,and $Nb_7Rh_6B_8$. High

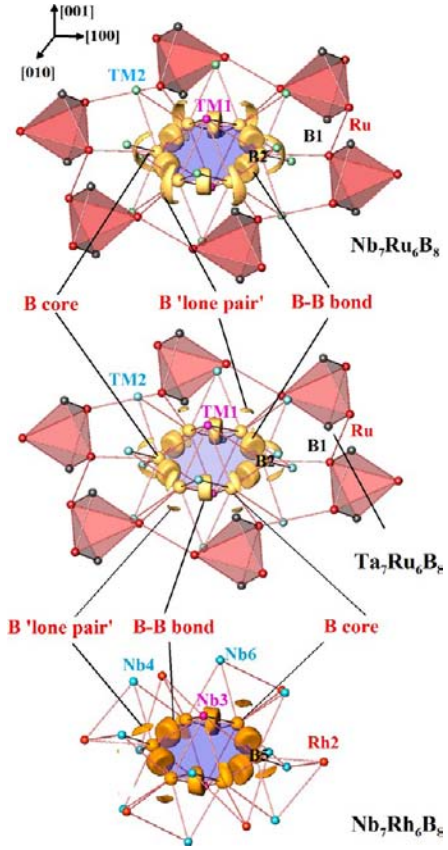

Figure 6. 1.286-localization domains of ELI-D (Y_D^α) for $Nb_7Ru_6B_8$ and $Ta_7Ru_6B_8$ and 1.300-localization domain of ELI-D for $Nb_7Rh_6B_8$ highlighting the bonding situation in the B_6 rings (violet). Red polyhedral Ru−B units are shown for $TM_7Ru_6B_8$ (see text).

localization of electrons is also found in the (spherical) core regions of the boron atoms. The localization domains between the B2 atoms in $Nb_7Ru_6B_8$ and $Ta_7Ru_6B_8$, as well as between the B1 and B2 atoms in $Nb_7Rh_6B_8$ (hereafter ring boron atoms), represent the B−B bonds within the ring. Substituting Rh for Ru does not change the topology of the ELI-D domains within the B_6 ring.

The domains curved around the boron cores of the ring and pointing toward the Ru or Rh atoms (forming the BTM'_6 trigonal prisms, of which, in Figure 6, only one Ru_3 basal plane with respective B atoms above and below are indicated by the red polyhedra for $TM_7Ru_6B_8$), could either represent a "lone-pair" of boron-ring atoms or stand for the *TM*′−B (and *TM*−B) bonding interaction.

The adherence of the curved ELI-D domains to the boron sites corroborates the idea of an enhanced lone-pair character of the electrons in the *TM*′−B region despite in $Nb_7Ru_6B_8$ the ELI-D attractors are located on the B−*TM*′ line. Further support for the lone-pair-like interpretation of the outer regions of the B_6 rings is found in the $Ta_7Ru_6B_8$ (Figure 6, middle). Here, instead of a single attractor on the Ru−B line, two attractors above and below the B_6 ring are observed. The additional argument for the lone-pair character of these attractors is found in $Nb_7Rh_6B_8$, where they are located out of the B_6 plane, and each boron atom has only one such attractor (Figure 6, bottom). Additionally, this is

dx.doi.org/10.1021/ic201978n | *Inorg. Chem.* 2012, 51, 7472−7483

supported by the DOS shown in Figure 4, manifesting mixing between the ring-B and Nb states instead of ring-B and Ru states. In the Ru compound, the ring−B−B bond basin is populated by 1.85 electrons and the lone-pair basin by 3.13 electrons. Attributing to each boron core basin of the B_6 ring a bond basin as well as a lone-pair basin yields the population of 7.09 electrons per such ring−B species in $Nb_7Ru_6B_8$.

It is possible to study the overlap of one of the lone-pair basins of the B_6 ring with the QTAIM atoms, applying the so-called intersection technique,[85−87] and determine how much of the lone-pair basin population belongs to the respective QTAIM atoms. For $Nb_7Ru_6B_8$ such a basin intersection shows, that only 0.34 electrons of the lone-pair basin (populated by 3.13 electrons) are inside the Ru QTAIM basin (0.37 electrons are inside the neighboring Nb2 QTAIM basins). The largest part of the 'lone-pair' population, 1.94 electrons, belongs to the ring-B QTAIM basins.

To understand these results, let us focus on the ELI-D distribution between the *TM*2 atoms. Lowering the ELI-D isovalues will increase the size of the localization domains. In case of $Nb_7Ru_6B_8$, at a sufficiently low ELI-D value, the localization domain of the B_6 unit fills up the region between the neighboring Nb2 cores (i.e., the Nb2−Nb2 regions are occupied by the ring−B lone-pair basins, Figure 7). This suggests rather B−*TM* instead

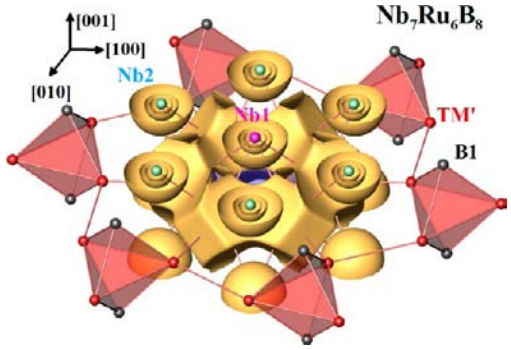

Figure 7. 1.02-localization domains of ELI-D (Y_D^α) for $Nb_7Ru_6B_8$.

of the B−*TM*′ interaction. It is worth noting that the basin sets corresponding to the Nb inner-shells are populated by roughly 38.0 electrons (i.e., yielding the charge +3.0), irrespective of the examined Rh compound or site, which is comparable with the charge +2.9 of the Nb core basin in NbB_2.

The analysis of the ELI-D distribution for $Ta_7Ru_6B_8$ yields results similar to the ones for the Nb compound. The most obvious difference is that the lone-pairs are characterized by two ELI-D maxima pointing between the closest Ta2 atoms (i.e., two separate lone-pair basins per boron atom). Additionally, the Ta core basins attain somewhat larger charge of roughly +3.4, that is, around 0.4 more than found for the Nb core basins. This is accompanied by slightly higher electron population (0.4 electrons) of the (two) lone-pairs attached to the B_6 rings.

Bonding in TM′$_6$B$_2$ Polyanion. Further inspection of ELI-D suggests the formation of a *TM*′$_6$B$_2$ framework in the examined compounds (Figure 8). In the valence region around the B1 core in $Nb_7Ru_6B_8$ (the corresponding basin is occupied by 2.07 electrons), three equal ELI-D domains are found, pointing to the *TM*′ atoms above and below (3-center interaction). Each of the corresponding valence basins is populated by 2.06 electrons in the Ru compound. The intersection of the valence basin with the QTAIM basins shows that the population of the ELI-D basin can

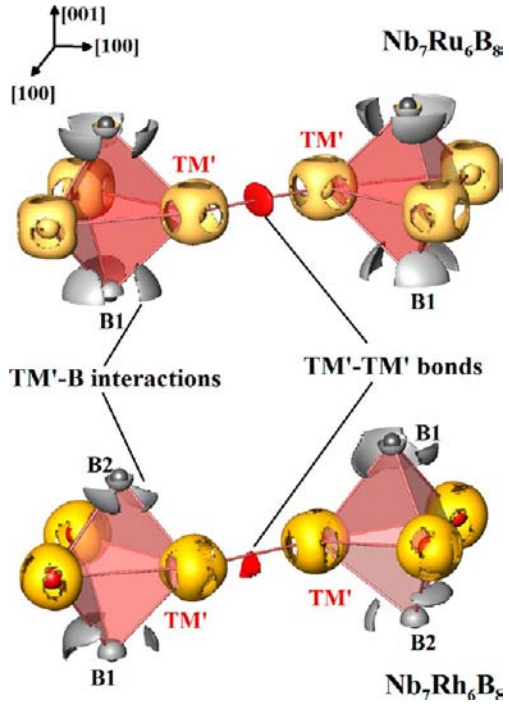

Figure 8. ELI-D (Y_D^α) for the *TM*′$_6$B$_2$ polyanions in $Nb_7TM'_6B_8$. The gray localization domains (Y_D^α = 1.345 for $Nb_7Ru_6B_8$ and Y_D^α = 1.23 for $Nb_7Rh_6B_8$) show the *TM*′−B−*TM*′ interactions, the orange localization domains (Y_D^α = 1.23 for $Nb_7Ru_6B_8$ and Y_D^α = 1.34 for $Nb_7Rh_6B_8$) highlight the structuring of the *TM*′ inner shells, and the red localization domains (Y_D^α = 0.992 for $Nb_7Ru_6B_8$ and Y_D^α = 0.966 for $Nb_7Rh_6B_8$) depict the *TM*′−*TM*′ interaction.

be ascribed to 50% to the nearest B1 atom. Thus, the B1 valence basins describe the *TM*′-B1 bonds (as can be also anticipated from the DOS (Figure 4) showing the mixing between the Ru and B1 states for $Nb_7Ru_6B_8$).

The structuring of the *TM*′ penultimate-shell in $Nb_7Ru_6B_8$ is characterized by the cubic arrangement of the ELI-D maxima. The basin set formed by the inner-shell basins is populated by 41.3 electrons, which corresponds to the charge of +2.7 (the same applies to the $Ta_7Ru_6B_8$ compound). The *TM*′$_6$B$_2$ units are interconnected by *TM*′−*TM*′ bonds, visualized by the red-colored localization domain in Figure 8. The corresponding (Ru−Ru bonding) basin is populated by 0.24 electrons (roughly the same is valid for the $Ta_7Ru_6B_8$ compound).

In the case of $Nb_7Rh_6B_8$, the additional electron of the *TM*′ atom causes changes in the *TM*′$_6$B$_2$ polyanion (Figure 8, bottom). Three equal three-center *TM*′−B−*TM*′ interactions split in 2+1. Thereby, two of these three bonds have rather a two-center character than the three-center one. Assuming that a 3*c* interaction is reflected by a longer *TM*′−B distance than a 2*c* one, this causes distortion of the trigonal prism (instead of six equal B−*TM*′ distances, four longer and two shorter are formed). The *TM*′ cannot be more located in one plane; thus this layer is puckered in Rh compounds. An additional interaction between Rh and Nb atoms appears.

Summarizing, the chemical bonding in the examined *TM*$_7$*TM*′$_6$B$_8$ compounds can be described as follows (Figure 9). The *TM* atoms are positively charged and play the role of the cations. The anionic substructure contains two types of polyanions: planar B_6 rings and three-dimensional *TM*′$_6$B$_2$ units. An additional *TM*−Rh interaction is observed in *TM*$_7$Rh$_6$B$_8$ compounds.

dx.doi.org/10.1021/ic201978n | *Inorg. Chem.* 2012, 51, 7472−7483

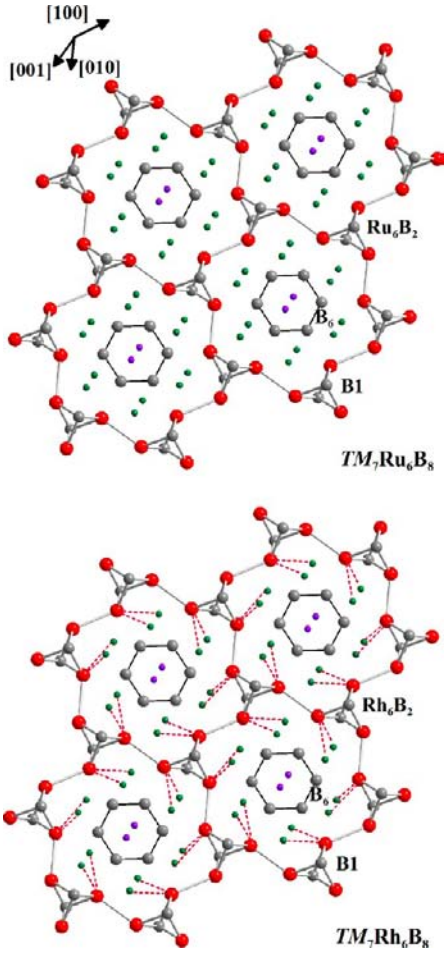

Figure 9. Atomic interactions in $TM_7TM'_6B_8$ compounds: gray lines connect the atoms in the polyanions, planar B_6 rings, and 3D TM'_6B_2 species; red lines show the additional *TM*−Rh interactions in $TM_7Rh_6B_8$ (*TM*, pink and green; *TM*′, red; boron, gray).

Physical Properties. The molar magnetic susceptibilities corrected for ferromagnetic contributions (corresponding to α-Fe contaminations between 2 and 28 ppm) are given in Figure 10. No phase transitions or superconductivity are observed. The weak upturn at the lowest temperatures is due to minor paramagnetic defects or impurities while the weak linear temperature dependence at high temperatures should be attributed to the Pauli-paramagnetic contribution. Using the increments for the closed shell ions, the diamagnetic contributions may be estimated.[87] Applying free-electron gas theory the electronic DOS at the Fermi levels can be calculated. For $Ta_7Ru_6B_8$ and $Nb_7Ru_6B_8$ we obtain 12.5 states eV^{-1} $f.u.^{-1}$ while for $Nb_7Rh_6B_8$ a value of 9.3 states eV^{-1} $f.u.^{-1}$ is calculated, in fair agreement with the DOS from the band structure calculations.

Because the compounds $Nb_7Ir_6B_8$ and $Ta_7Ir_6B_8$ could not be obtained as single phases, the measured samples contained the impurity phases $TMIr_3$, Nb_3B_4, and TaB. Both samples $Nb_7Ir_6B_8$ and $Ta_7Ir_6B_8$ show diamagnetic behavior in the studied temperature range (Figure 10). The amounts of impurities are not large and taking in account large negative contributions of iridium, it may be concluded that the Ir compounds are intrinsic diamagnets.

The electrical resistivity $\rho(T)$ of the sample $Ta_7Ru_6B_8$ (Figure 11) is high and only weakly temperature dependent. The high residual resistivity ρ_0 of ≈10.3 μΩ m is probably due to microcracks in the polycrystalline sample. The temperature-dependent part shows a typical metallic characteristic and its increase ($\rho_{300} - \rho_0 \approx 1.2\ \mu\Omega$ m) is of the order often observed for ternary intermetallic compounds.

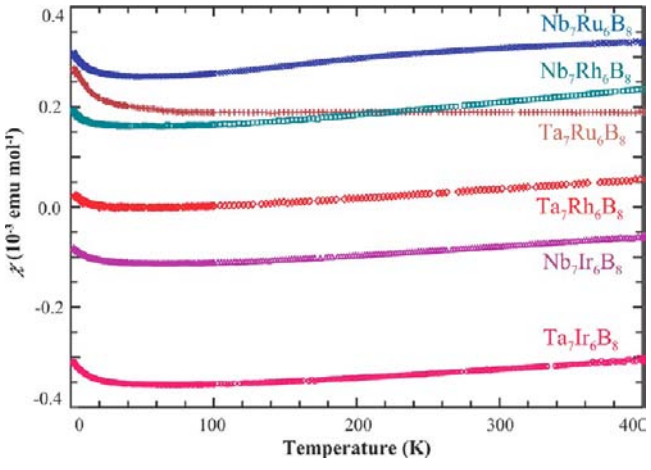

Figure 10. Magnetic susceptibility $\chi(T)$ of samples of the $TM_7TM'_6B_8$ compounds (*TM* = Ta, Nb; *TM*′ = Ru, Rh, Ir).

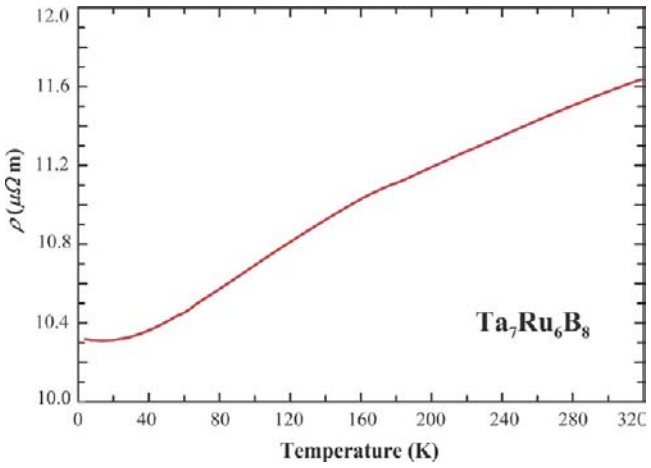

Figure 11. Temperature dependence of the electrical resistivity (ρ) for $Ta_7Ru_6B_8$.

CONCLUSIONS

In this work, we report on new ternary borides $TM_7TM'_6B_8$ (*TM* = Nb, Ta; *TM*′ = Ru, Rh, Ir). They crystallize with an ordered antitype to $Ce_7In_6Ni_{5\pm x}Ge_{3\pm x}$. This atomic arrangement, closely related to AlB_2, is for the first time observed for the intermetallic borides and is characterized by formation of planar B_6 rings. Electronic structure calculations within the TB-LMTO-ASA approach, as well as measurements of physical properties, show the metallic character of the new compounds. Magnetic susceptibility measurements reveal $TM_7TM'_6B_8$ (*TM* = Nb, Ta; *TM*′ = Ru, Rh) to be Pauli paramagnets, while Ir-containing compounds are essentially diamagnetic.

Quantum-chemical analysis of the chemical bonding in the $TM_7TM'_6B_8$ compounds within the electron density/electron localizability approach reveals the *TM* atoms forming a cationic substructure with separated cations. The anionic part of the

dx.doi.org/10.1021/ic201978n | Inorg. Chem. 2012, 51, 7472−7483

structure contains two polyanions: planar B_6 rings and a three-dimensional TM'_6B_2 framework. An additional TM−Rh interaction is present in $TM_7Rh_6B_8$ compounds. The differences of atomic interactions between Rh and Ru compounds were explained by application of electron-localizability tools.

AUTHOR INFORMATION

Corresponding Author

*Email: grin@cpfs.mpg.de.

Notes

The authors declare no competing financial interest.

Upon completion of the revised version of this contribution we became aware of a recent study of $Ti_7Rh_4Ir_2B_8$,[88] which forms a superstructure to $TM_7Ru_6B_8$ with the same shape of unit cell and ordered occupations of Ru positions with Rh and iridium.

ACKNOWLEDGMENTS

Qiang Zheng acknowledges support by the CAS-MPG Partner Group at Shanghai Institute of Ceramics.

REFERENCES

(1) Matkovich, V. I. *Boron and Refractory Borides*; Springer: New York, 1977.
(2) Thompson, R. *J. Less-Common Met.* **1976**, *47*, 279.
(3) Schwarzkopf, P.; Kieffer, R.; Leszynski, W.; Benesovsky, K. *Refractory Hard Metals, Borides, Carbides, Nitrides, and Silicides*; Macmillan: New York, 1953.
(4) Munro, R. G. *J. Res. Natl. Inst. Stand. Technol.* **2000**, *105*, 709.
(5) Guo, S. Q. *J. Eur. Ceram. Soc.* **2009**, *29*, 995.
(6) Samsonov, G. V.; Vinitskii, I. M. *Handbook of Refractory Compounds*; IFI/Plenum: New York, 1980.
(7) Buzea, C.; Yamashita, T. *Supercond. Sci. Technol.* **2001**, *14*, R115.
(8) Levine, J. B.; Tolbert, S. H.; Kaner, R. B. *Adv. Funct. Mater.* **2009**, *19*, 3519.
(9) Upadhya, K. *Am. Ceram. Soc. Bull.* **1997**, *76*, 51.
(10) Rogl, P.; Nowotny, H. *J. Less-Common Met.* **1978**, *61*, 39.
(11) Nowotny, H.; Rogl, P. In *Boron and Refractory Borides*; Matkovich, V. I., Ed.; Springer: New York, 1977.
(12) Kuzma, Yu.B. *Crystallochemistry of Borides*; Lviv University Publishers: Lviv, 1983.
(13) Kuzma, Yu.B.; Chaban, N. F. *Binary and Ternary Systems Containing Boron*; Metallurgiya: Moscow, 1990.
(14) Rogl, P. In *Inorganic Reactions and Methods*; Hagen, A. P., Ed.; Wiley: 1991.
(15) Albert, B.; Hillebrecht, H. *Angew. Chem., Int. Ed.* **2009**, *48*, 8640.
(16) Mori, T. In *Handbook on the Physics and Chemistry of Rare-Earths*; Gschneidner, K. A.; Jr., Bunzli, J.-C.; , Pecharsky, V., Eds.; North-Holland: Amsterdam, 2008; Vol. *38*, p 105.
(17) Lundström, T. *Ark. Kemi* **1969**, *31*, 227.
(18) Rogl, P. *J. Less-Common Met.* **1985**, *110*, 283.
(19) Ku, H. C.; Yu, H. *Phys. Rev. B* **1986**, *34*, 1974.
(20) Isnard, O.; Fruchart, D. *J. Alloys Compd.* **1994**, *205*, 1.
(21) Dronskowski, R.; Korczak, K.; Lueken, H.; Jung, W. *Angew. Chem., Int. Ed.* **2002**, *41*, 2528.
(22) Gignoux, D.; Schmitt, D. In *Handbook of Magnetic Materials*; Buschow, K. H. J., Ed.;North-Holland: Amsterdam, 1997; Vol. *10*, p239.
(23) Matthias, B. T.; Corenzwit, E.; Vandenberg, J. M.; Barz, H. E. *Proc. Natl. Acad. Sci. U.S.A.* **1997**, *74*, 1334.
(24) Vandenberg, J. M.; Matthias, B. T.; Corenzwit, E.; Barz, H. *Mater. Res. Bull.* **1975**, *10*, 889.
(25) Ku, H. C.; Meisner, G. P.; Acker, F. *Solid State Commun.* **1980**, *35*, 91.
(26) Nagamatsu, J.; Nakagawa, N.; Muranaka, T.; Zenitani, Y.; Akimitsu, J. *Nature* **2001**, *410*, 63.
(27) Maple, M. B. *AIP Conf. Proc.* **1991**, *231*, 165.
(28) Werheit, H. *Mater. Sci. Eng. B* **1995**, *29*, 228.
(29) Mori, T. *J. Phys.: Conf. Ser.* **2009**, *176*, 012036.
(30) Mori, T.; Nishimura, T. *J. Solid State Chem.* **2006**, *179*, 2908.
(31) Maple, M.; Lambert, S.; Torikachvili, M.; Yang, K.; Allen, J.; Pate, B.; Lindau, L. *J. Less-Common Met.* **1985**, *111*, 239−249.
(32) Prasad, A.; Hossain, Z.; Jeevan, H.; Geibel, C. *J. Phys.: Cond. Mat.* **2009**, *21*, 206003.
(33) Yatskar, A.; Budraa, N.; Beyermann, W.; Canfield, P.; Budko, S. *Phys. Rev. B* **1996**, *54*, 3772.
(34) Herbst, J. *Rev. Mod. Physics* **1991**, *63*, 819.
(35) Inoue, A. *Acta Mater.* **2000**, *48*, 279−306.
(36) Lafferty, J. *J. Appl. Phys.* **1951**, *22*, 299−309.
(37) Champagne, B.; Dallaire, S. *J. Vac. Sci. Technol. A* **1985**, *3*, 2373−2377.
(38) Sigl, L.; Schwetz, K. *Powder Metall. Int.* **1991**, *23*, 221−224.
(39) Takagi, K. *J. Solid State Chem.* **2006**, *179*, 2809.
(40) Leithe-Jasper, A.; Klesnar, H.; Rogl, P.; Komai, M.; Takagi, K. *J. Jpn. Inst. Met.* **2000**, *64*, 154.
(41) Yu, H.; Zheng, Y.; Liu, W.; Pang, X.; Zheng, J.; Xiong, W. *Int. J. Refractory Hard Mater.* **2010**, *28*, 338.
(42) Haschke, H.; Nowotny, H.; Benesovsky, F. *Mh. Chem* **1966**, *97*, 1459.
(43) Rieger, W.; Nowotny, H.; Benesovsky, F. *Mh. Chem.* **1965**, *96*, 844.
(44) Rogl, P.; Nowotny, H.; Benesovsky, F. *Mh. Chem.* **1972**, *103*, 965.
(45) Rogl, P.; Nowotny, H.; Benesovsky, F. *Mh.Chem.* **1970**, *101*, 850.
(46) Rogl, P.; Nowotny, H. *Mh. Chem.* **1973**, *104*, 943.
(47) Rogl, P.; Nowotny, H.; Benesovsky, F. *Mh.Chem.* **1971**, *102*, 678.
(48) Rogl, P.; Rudy, E. *J. Solid State Chem.* **1978**, *24*, 175.
(49) Jung, W. *J. Less-Common Met.* **1984**, *97*, 253.
(50) Kotzott, D.; Ade, M.; Hillebrecht, H. *Solid State Sci.* **2008**, *10*, 291.
(51) Misse, P.; Fokwa, B. *Z. Anorg. Allg. Chem.* **2010**, *636*, 1013.
(52) Fokwa, B. *Eur. J. Inorg. Chem.* **2010**, *20*, 3075.
(53) Alekseeva, A.; Abakumov, A.; Chizhov, P.; Leithe-Jasper, A.; Schnelle, W.; Prots, Y.; Hadermann, J.; Antipov, E.; Grin, Y. *Inorg. Chem.* **2007**, *46*, 7378.
(54) Veremchuk, I.; Mori, T.; Prots, Y.; Schnelle, W.; Leithe-Jasper, A.; Kohout, M.; Grin, Y. *J. Solid State Chem.* **2008**, *181*, 1983.
(55) Zheng, Q.; Gumeniuk, R.; Borrmann, H.; Burkhardt, U.; Schnelle, W.; Leithe-Jasper, A.; Grin, Y. *17th International Symposium on Boron, Borides, and Related Materials, Istanbul* **2011**, 201.
(56) *WinXPow*, version 2; STOE and Cie GmbH: Darmstadt, 2001.
(57) Akselrud, L.; Zavalii, P.; Grin, Y.; Pecharsky, V.; Baumgartner, B.; Wölfel, E. *Mater. Sci. Forum* **1993**, *335*, 133.
(58) Rodriguez-Carvajal, J. J. *Phys. B* **1993**, *192*, 55.
(59) Jepsen, O.; Burkhardt, A.; Andersen, O. K. *TB-LMTO-ASA*, version 4.7; Max-Planck-Institut für Festkörperforschung: Stuttgart, Germany, 1999.
(60) Kohout, M. *Int. J. Quantum Chem.* **2004**, *97*, 651.
(61) Kohout, M.; Wagner, F. R.; Grin, Y. *Int. J. Quantum Chem.* **2006**, *106*, 1499.
(62) Kohout, M. *DGrid*, version 4.6; Max-Planck-Institut für Festkörperforschung: Stuttgart, Germany, 2011.
(63) Bader, R. F. W. *Atoms in Molecules*; Oxford University Press: Oxford, 1990.
(64) Steurer, W.; Rogl, P.; Nowotny, H. *Mh. Chem.* **1979**, *110*, 791.
(65) Kiessling, R. *Acta Chem. Scand.* **1949**, *3*, 603.
(66) Spear, K.; Gilles, P. *High Temp. Sci.* **1969**, *1*, 86.
(67) Grin, Y.; Gladyshevski, R. *Gallides*; Nauka: Moscow, 1984.
(68) Gladyshevski, E. I.; Grin, Yu. *Kristallografia* **1981**, *26*, 1204; *Sov. Phys. Crystallogr.* **1981**, *26*, 683.
(69) Pöttgen, R.; Gravereau, P.; Darriet, B.; Chevalier, B.; Hickey, E.; Etourneau, J. *J. Mater. Chem.* **1994**, *4*, 463−467.
(70) Cardoso-Gil, R.; Carillo-Cabrera, W.; Schultheiss, M.; Peters, K.; von Schnering, H. G.; Grin, Y. *Z. Anorg. Allg. Chem.* **1999**, *625*, 1.
(71) Yarmoliuk, Y.; Akselrud, L. *Kristallographiya* **1983**, *28*, 1111.
(72) Chumalo, N.; Nychyporuk, G.; Pavlyuk, V.; Pöttgen, R.; D. Kaczorowski, D.; Zaremba, V. *J. Solid State Chem.* **2010**, *183*, 2963.
(73) Yarmoliuk, Y.; Grin, Y.; Gladyshevski, E. *Dopov. Akad. Nauk URSR, Ser. A* **1978**, *9*, 855.

(74) Grin, Y.; Yarmoliuk, Y. *Visnyk Lviv. Univ. ser. Chem.* **1979**, *21*, 13–17.
(75) Emsley, J. *The Elements*; Clarendon Press: Oxford, 1998.
(76) Okada, S.; Hamano, K.; Lundstrom, T.; Higashi, I. *AIP Conf. Proc.* **1991**, *231*, 456.
(77) Okada, S.; Kudou, K.; Higashi, I.; Lundstrom, T. *J. Cryst. Growth* **1993**, *128*, 1120.
(78) Kuzma, Y. *Dopov. Akad. Nauk URSR, ser. A* **1967**, *1967*, 939.
(79) Kripyakevich, P.; Kuzma, Y.; Voroshilov, Y.; Brink-Shoemaker, C.; Shoemaker, D. *Acta Cryst. B* **1971**, *27*, 257.
(80) Kuzma, Y.; Kripyakevich, P.; Chepiga, M. *Zhurnal Strukturnoi Khimii* **1968**, *9*, 327.
(81) Pendás, M. A.; Blanco, M. A.; Costales, A.; Mori Sánches, P.; Luaña, V. *Phys. Rev. Lett.* **1999**, *83*, 1930.
(82) Shein, I.; Ivanovskii, A. *Phys. Rev. B* **2006**, *73*, 144108.
(83) Tsirelson, V.; Stash, A.; Kohout, M.; Rosner, H.; Mori, H.; Sato, S.; Lee, S.; Yamamoto, A.; Tajima, S.; Grin, Y. *Acta Crystallogr. B* **2003**, *59*, 575.
(84) Wagner, F. R.; Bezugly, V.; Kohout, M.; Grin, Y. *Chem.—Eur. J.* **2007**, *13*, 5724.
(85) Jansen, G.; Schubert, M.; Findeis, B.; Gade, L. H.; Scowen, I., J.; McPartlin, M. *J. Am. Chem. Soc.* **1998**, *120*, 7239.
(86) Raub, S.; Jansen, G. *Theor. Chem. Acc.* **2001**, *106*, 223.
(87) Selwood, P. *Magnetochemisty*; Interscience: New York, 1956.
(88) Fokwa, B. P. T.; Hermus, M. *Angew. Chem.* **2012**, *124*, 1734.